

Single-particle motion in liquid sodium

C. Morkel and W. Gläser

Physik-Department, Technische Universität München, D-8046 Garching bei München, Federal Republic of Germany

(Received 16 July 1985)

The van Hove scattering function $S(Q, \omega)$ of liquid sodium has been measured at three states in the temperature range 400 to 800 K for magnitudes of the scattering vector Q between 0.3 and 4.6 \AA^{-1} . Coherent and incoherent scattering were separated by a model analysis. The incoherent data were analyzed in terms of a collision rate and several shape parameters of $S_s(Q, \omega)$ such as the reduced half-width $\gamma(Q) = \omega_{1/2}(Q)/(DQ)^2$. Results were compared with a kinetic-model theory of Götze and Zippelius, showing good agreement. The observed resonancelike transition of $\gamma(Q)$ from a diffusive to a more "hard-sphere-gas"-like behavior is temperature dependent and indicates no simple relation to the static structure factor of the liquid.

I. INTRODUCTION

Much of our present knowledge of diffusion or single-particle motion in liquid metals was collected over the last two decades.¹ Besides tracer methods and NMR techniques, the usefulness of neutron scattering techniques for experimental investigations of diffusive motions has also been recognized.

Whereas the former techniques essentially yield information on the Brownian limit of diffusion, inelastic scattering of slow neutrons in principle can explore the entire time and space range of atomic motions. Early neutron scattering experiments^{2,3} demonstrated these possibilities but suffered from technical limitations and statistical accuracy.

Recent progress in our understanding of single-particle motion in liquids mainly came through computer simulations^{4,5,6} and the development of kinetic theories.^{7,8} Especially the analysis of the molecular-dynamics data for the incoherent scattering function $S_s(Q, \omega)$ showed, besides the well-known limits of Brownian diffusion for $Q \rightarrow 0$ and perfect-gas behavior for $Q \rightarrow \infty$, interesting changes in the shape of this function in the intermediate- Q range, which subsequently were qualitatively explained by improved kinetic models.⁷ These advances in theory suggested more detailed neutron scattering studies especially in the intermediate- Q range. In this paper we report the results of a series of neutron scattering measurements on liquid sodium in the temperature range from 400 to 800 K, which support the kinetic-model analysis in the low- and intermediate- Q regions but show systematic deviations at larger Q .

In Sec. II the experimental technique will be described. Section III outlines the data analysis and describes the models used to represent the experimental data and the corrections necessary to determine the incoherent part of the scattering function. Although coherent and incoherent scattering on sodium can be separated model independently by the use of neutron polarization analysis, a technique which we will describe in a later paper, in this work a simple model for coherent scattering described by Lovesey⁹ has been used. The data analysis was further

simplified by making use of the observation that the incoherent data can be represented in good approximation by the Nelkin-Ghatak model¹⁰ using a Q -dependent effective collision rate. Finally, the essential results of this analysis of the experimental data are presented and compared to theoretical models in Sec. IV.

II. EXPERIMENTAL DETAILS

A. Samples

Liquid sodium samples of high purity (99.95%) were held in cylindrical vanadium tubes of 15.1-mm inner diameter, 0.2-mm wall thickness, and 150-mm length, allowing for thermal expansion of the sodium between the melting point ($T_{\text{mp}} = 371$ K) and 1000 K. The liquid sodium density $\rho_{\text{mp}} = 0.927$ g/cm³ and the free cross sections¹¹ of sodium for coherent scattering ($\sigma_f^c = 1.54$ b), incoherent scattering ($\sigma_f^{\text{inc}} = 1.55$ b) and absorption of neutrons ($\sigma^a = 0.53$ b, $\lambda = 1.8$ Å) cause roughly 10% scattering of the incident neutron beam in the temperature range of the experiment. For heating the samples to the temperatures requested the spectrometers IN4 and IN6 at the Institut Laue-Langevin (ILL) used for the scattering experiments were equipped with standard vacuum furnaces. The spectrometers and auxiliary equipment are described elsewhere.¹² Scattering runs were performed at temperatures of the sodium samples of 403, 602, and 803 K. The temperature was controlled by two W-Rh thermocouples indicating a temperature stability of ± 1 K and a temperature homogeneity along the total sample length of the order of 1%.

B. Measurements

Neutron time-of-flight spectra were taken on both spectrometers mentioned above. The spectrometer IN4 is a phased rotating crystal spectrometer using two graphite crystals. It was operated at an incident neutron energy $E_0 = 12.55$ meV with an elastic energy resolution of 0.57 meV. The 228 ³He counters (each 1 inch in diameter and 12 inches in length) were placed at a distance of 4.02 m from the sample on a vertical arc covering an angular

range from 9° to 139.5° . In this way elastic scattering vectors from 0.3 to 4.6 \AA^{-1} could be measured. To adjust the Q resolution, at different angles different numbers of counters were grouped together and between 9° and 18° the active length of the counters was reduced to 6 inches. The time-of-flight data for each detector position were recorded into 256 time channels each of $16 \mu\text{sec}$.

IN6 which is a focusing crystal chopper spectrometer was operated at an incident energy $E_0 = 2.35 \text{ meV}$ with an elastic energy resolution of 0.053 meV , thus allowing measurements in the low- Q region with an order of magnitude improved resolution. At this instrument with a flight path of 2.47 m an angular range from 17.3° to 103.6° was covered with groups of ^3He counters (elliptic cross section $15 \times 30 \text{ mm}$, 12 inches in length), including seven counters at the smallest and 18 counters at the largest scattering angle. From these geometrical data a Q resolution of 0.02 \AA^{-1} is deduced for the smallest scattering angle. At IN6 time-of-flight data for each detector position were recorded in 256 time channels of $14 \mu\text{sec}$. The kinematic region covered by both instruments is illustrated in Fig. 1. For both instruments the resolution function was determined from elastic scattering on vanadium. Because the vanadium data were also used for normalizing the sodium scattering data the vanadium sample was constructed as a spiral to match the sodium sample in geometry and scattering power (atomic number density is $1.49 \times 10^{22} \text{ cm}^{-3}$). The sample alignment was checked by using a cadmium rod of the same size in place of the sample.

Besides sample (sodium) runs at the three temperatures mentioned, empty container runs (empty vanadium container and furnace) and empty furnace runs were performed at the same temperatures in order to supply information for quantitative corrections of the sample environment contribution to the recorded scattering.

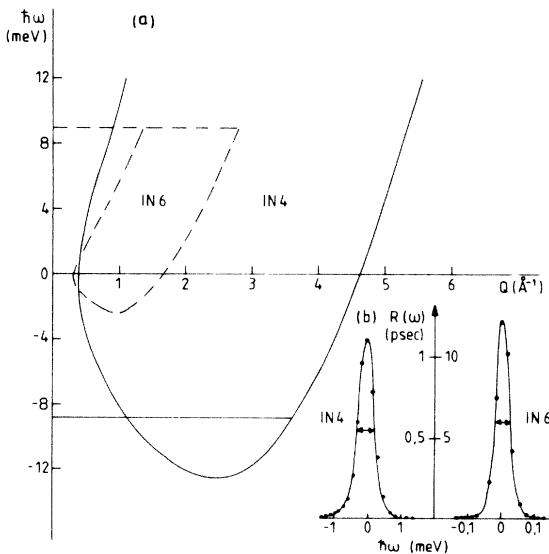


FIG. 1. (a) Kinematic region of the used instruments IN4 ($E_0 = 12.55 \text{ meV}$, solid curve) and IN6 ($E_0 = 2.35 \text{ meV}$, dashed curve). (b) Experimental resolution function for IN4 ($\Delta E = 0.57 \text{ meV}$) and IN6 ($\Delta E = 0.053 \text{ meV}$).

III. DATA EVALUATION AND MODEL DESCRIPTION

A. Intensity attenuations and background corrections

The relatively strong sample environment scattering required careful corrections, especially for the contributions of the container and the furnace to the total scattering. In a typical detector in the low- Q region a total of 6×10^5 counts were collected, of which about 30% originates from the sample environment. The standard procedure¹³ to treat container scattering was extended to include the contribution of the furnace. The scattering from the sodium sample was calculated using the following expression:¹⁴

$$I_s(\theta, \omega) = \frac{1}{A_{\text{SSCF}}(\theta, \omega)} \times \left[I_{\text{SCF}}(\theta, \omega) - \frac{A_{\text{CSCF}}(\theta, \omega)}{A_{\text{CCF}}(\theta, \omega)} I_{\text{CF}}(\theta, \omega) - \left[\frac{A_{\text{FSCF}}(\theta, \omega)}{A_{\text{FF}}(\theta, \omega)} - \frac{A_{\text{CSCF}}(\theta, \omega)}{A_{\text{CCF}}(\theta, \omega)} \right] \times \frac{A_{\text{FCF}}(\theta, \omega)}{A_{\text{FF}}(\theta, \omega)} \right] I_{\text{F}}(\theta, \omega) \quad (1)$$

The attenuation factors A_{SSCF} , etc. (S, C, and F mean sample, container, and furnace in the notation of Paalman and Pings¹³), were calculated numerically as a function of scattering angle and energy transfer, taking the actual beam geometry (e.g., diaphragms) of each experiment into account. The so-evaluated sample scattering then was normalized per number of atoms and unit solid angle and further reduced to an effective symmetric scattering function

$$\hat{S}_{\text{eff}}(\theta, \omega) = \frac{4\pi}{\sigma_s} \frac{k_0}{k} \frac{I'_s(\theta, \omega)}{f(k)} e^{\hbar\omega/2k_B T}, \quad (2)$$

where $I'_s(\theta, \omega)$ is the sample scattering per atom, unit solid angle, and energy interval and $f(k)$ is the detector efficiency for wave number k , which was derived from the vanadium data.

B. Conversion to constant wave-vector transfer

For the discussion of results and comparison with models it is sometimes more convenient to have the data at constant momentum transfer $\hbar Q$, therefore the $\hat{S}_{\text{eff}}(\theta, \omega)$ data were sorted for the given elastic Q values of the detector using a ΔQ window corresponding to the instrumental Q resolution. Because experimental data are available only along discrete paths $\theta = \text{const}$ in the kinematic plane, this sorting leads to an incomplete covering of the $\hat{S}(Q, \omega)$ distribution on the ω scale. A two-dimensional interpolation would remove this feature, but we considered it more reliable to base further discussions on directly available experiment data.

C. Multiple-scattering corrections

The raw data are the sum of singly and multiply scattered neutrons. In principle the multiple-scattering component may be removed by simulating the experiment with a Monte Carlo technique.¹⁵ However, in the present case we felt that a simpler approach would suffice, namely an estimation of sodium multiple scattering using an effective mass gas model [$M_{\text{eff}} = MS(Q)$] for the dynamic effects and adjusting the magnitude of the necessary correction to the experimental remaining background at large energy transfer. This gives the phenomenological prescription with Q_0 the position of the maximum of $S(Q)$,

$$\Delta_m(\omega) = \frac{\Delta_0}{\sqrt{2\pi}Q_{\text{eff}}v_0} \exp\left[-\frac{\omega^2}{2Q_{\text{eff}}^2v_0^2}\right], \quad (3)$$

$$v_0^2 = k_B T/M, \quad Q_{\text{eff}} = Q_0/[S(Q_0)]^{1/2}.$$

Using the tables of Ref. 16 gave $\Delta_0 = 0.08$ for the actual sample geometry. The experimental background suggested a slightly higher value $\Delta_0^{\text{expt}} \approx 0.1$ which can be justified by additional multiple-scattering contributions of the sample environment. Because multiple scattering is a rather broad structureless distribution, small changes in Q_{eff} in Eq. (3) will have only a minor influence on the parameters of single scattering to be determined.

D. Model analysis

The main aim of the present investigation is the analysis of the incoherent part of the scattering. Sodium scatters neutrons both coherently and incoherently with about equal strength. The reduced data $\hat{S}_{\text{eff}}(Q, \omega)$ have to be written in the following form:

$$\hat{S}_{\text{eff}}(Q, \omega) = \frac{\sigma_c}{\sigma_s} \hat{S}(Q, \omega) + \frac{\sigma_i}{\sigma_s} \hat{S}_s(Q, \omega) + \Delta_m(\omega). \quad (4)$$

Because in the present measurements an experimental separation of coherent and incoherent scattering was not possible, a separation based on model description was tried. An essential coherent contribution to total scattering occurs in the region of the maximum of the static structure factor $S(Q)$ around Q_0 .

It is believed that for this Q region and extending to greater Q values the "viscoelastic model" of Lovesey⁹ may be a reasonable approximation for our purpose. This was confirmed in a preliminary polarization analysis experiment on the spectrometer D7B at the ILL¹⁷ which allows a model-independent separation of coherent and incoherent scattering. The analysis of the coherent part of these data yield relaxation times $\tau(Q)$, which agree within an uncertainty limit of about 10% with the values calculated with the ansatz of Lovesey. Therefore in the analysis of our data the coherent scattering contribution was represented by the following model:

$$S(Q, \omega) = \frac{S(Q)}{\pi} \frac{\omega_0^2(\omega_i^2 - \omega_0^2)\tau(Q)}{(\omega^2 - \omega_0^2)^2 + [\omega\tau(Q)(\omega^2 - \omega_i^2)]^2}, \quad (5)$$

where

$$\omega_0^2 = \frac{k_B T Q^2}{MS(Q)}, \quad \tau(Q) = \frac{1}{2} \left[\frac{\pi}{\omega_i^2 - \omega_0^2} \right]^{1/2}$$

and

$$\omega_i^2 = \frac{3k_B T Q^2}{M} + \omega_E^2 \left[1 - \frac{3 \sin(Qr_0)}{Qr_0} - \frac{6 \cos(Qr_0)}{(Qr_0)^2} + \frac{6 \sin(Qr_0)}{(Qr_0)^3} \right],$$

ω_i^2 is the ratio of fourth to second moment, ω_E the Einstein frequency, and r_0 the radius of the pair correlation maximum. It should be noted that (5) satisfies the sum rules up to the fourth moment.

The $S(Q)$ data of the present experiment which we used in Eq. (5) are illustrated in Fig. 2. At 403 K where a comparison with x-ray data¹⁸ is possible, a reasonable agreement is found with the exception of the low- Q region, where we believe our multiple-scattering correction may be insufficient. The numbers used for radius r_0 (Ref. 19) and Einstein frequency ω_E (Ref. 19) are given in Table I. As values for ω_E of sodium are available only at 400 K the numbers at 602 and 803 K were extrapolated using the suggested scaling relation²⁰ $\omega_E^2 \approx \sqrt{T} n^2(T)$, where $n(T)$ is the number density.

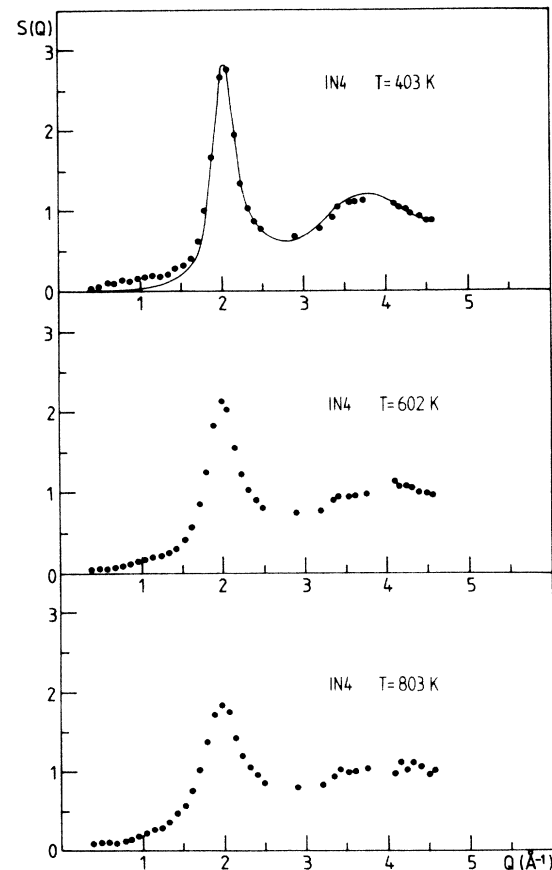


FIG. 2. Structure factor of liquid sodium at three temperatures. For comparison, x-ray data (Ref. 18) for $T = 373$ K are included (solid curve).

TABLE I. Parameters used for the viscoelastic model of sodium and values for the diffusion constant D (Ref. 1).

T (K)	r_0 (Å)	ω_E (10^{12} s $^{-1}$)	D (10^{-5} cm 2 s $^{-1}$)
403	3.4	16.2	5.0
602	3.4	17.0	12.8
803	3.3	17.2	22.0

One shortcoming of the model (5) is that it does not describe the perfect-gas limit properly. Therefore this description was improved in the higher ω region by the so-called Sköld approximation,²¹ which shows perfect-gas behavior $S_{\text{pg}}(Q, \omega)$ for the scattering law at high Q ,

$$S(Q, \omega) = S(Q)S_{\text{pg}}(Q', \omega), \quad (6)$$

$$Q' = Q/[S(Q)]^{1/2} \quad (\omega > 2\omega_E).$$

The formula (6) was used for $\omega > 2\omega_E$, as for these high energies ($\simeq 20$ meV) the statistical accuracy of the data does not allow us to distinguish between different models. Our model description approach in the analysis of the sodium data also suggested searching for a simple model to parameterize the incoherent part of the scattering. We found a single relaxation-time solution of the linearized Boltzmann equation described first by Nelkin and Ghatak¹⁰ convenient for this purpose. The Nelkin-Ghatak model can be summarized as follows:

$$S_s(Q, \omega) = \frac{1}{\pi\alpha} \frac{U(1-U) - V^2}{(1-U)^2 + V^2}, \quad (7)$$

where $U(x, y) = \sqrt{\pi}yu(x, y)$, $V(x, y) = \sqrt{\pi}yv(x, y)$, and $W(x + iy) = u(x, y) + iv(x, y)$ is the probability function for complex argument.²²

The reduced variables are defined as

$$x = -\frac{\omega}{\sqrt{2}Qv_0}, \quad y = \frac{\alpha}{\sqrt{2}Qv_0}. \quad (8)$$

The only parameter of this simple binary collision model is the collision parameter α or y . The model is attractive because it yields both the exact low- Q and high- Q limits of the incoherent scattering function. For $Q \rightarrow 0$, i.e., $y \gg 1$ with v_0^2/α set equal to the diffusion constant D , (7) reduces to the Lorentzian for classical diffusion and for $Q \rightarrow \infty$, i.e., $y \rightarrow 0$, (7) reduces to the perfect-gas scattering function.

A binary collision model is certainly too simple to give a realistic description of liquid dynamics. However, in a parameterized analysis approach a discussion of an experimentally determined effective Q -dependent collision parameter $\alpha(Q)$ may give valuable quantitative information on the improvements necessary in a more realistic theory.

A similar but more phenomenological model proposed by Egelstaff and Schofield²³ could also be used in the type of analysis suggested.

E. Resolution correction

In the low- Q region covered by the present experiment the width of the (mainly incoherent) scattering function became comparable with the resolution width of the spectrometers which made a proper correction mandatory. The resolution functions of both instruments (IN4, IN6) were deduced from the measured vanadium data, an example of which is given in Fig. 1, by fitting a cubic spline to these data.

Finally, the ansatz (4) including the described models for coherent and incoherent scattering was folded with the experimentally determined resolution and the resulting expression was fitted to the experimental data by a nonlinear least-squares fit technique.

The essential parameter determined in this way, namely $\alpha(Q)$, corresponds to that of the resolution corrected incoherent scattering function. The results for $\alpha(Q)$ and other derived quantities like the reduced half-widths $\gamma(Q) = \omega_{1/2}(Q)/DQ^2$ and $\Delta(Q) = 2\omega_{1/2}(Q)S(Q, 0)$ will be discussed in the next section.

IV. RESULTS AND DISCUSSION

Figure 3 shows some examples of incoherent scattering functions derived in the described way from the measured time-of-flight spectra. Although all these scattering functions are smooth bell-shaped curves as functions of ω , a closer inspection of their shape seems to indicate a change from a more Lorentzian-like to a more Gaussian-like behavior. A simple quantitative description of this observation can be given by the product of the width and the maximum peak height:²⁴ $\Delta(Q) = 2\omega_{1/2}\hat{S}_s(Q, 0)$. For normalized scattering functions $\hat{S}_s(Q, \omega)$ this product is $\Delta_L(Q) = 2/\pi$ in the case of a pure Lorentzian, whereas it is $\Delta_G(Q) = (4 \ln 2/\pi)^{1/2}$ for a Gaussian.

In Fig. 4 the evaluated values of $\Delta(Q)$ for the measured $\hat{S}_s(Q, \omega)$ of liquid sodium at the three temperatures investigated are plotted versus Q . At $T = 403$ K, which is close to the melting point, the crossover from Lorentzian to Gaussian behavior is rather smooth; it starts essentially at $Q > 2.5$ Å $^{-1}$ and is still not completed at the end of the experimental Q range. At the higher temperatures the "step" in $\Delta(Q)$ clearly is more pronounced and seems to shift to lower Q with increasing T . Although in the limit $Q \rightarrow \infty$ $\hat{S}_s(Q, \omega)$ has to be Gaussian, the observation that the transition occurs already at intermediate Q and in a relatively narrow Q range is surprising.

This change in shape also is reflected in the Q dependence of the effective collision rate $\alpha(Q)$ introduced in Sec. III. In Fig. 5 the results of the least-squares fits for $\alpha(Q)$ are shown. In the low- Q region $\alpha(Q)$ is nearly independent of Q and its numerical value is in good agreement with $\alpha_0 = v_0^2/D$ calculated with the known diffusion constant¹ at the corresponding temperature.

In the same Q range where $\Delta(Q)$ increases, the collision rate sharply decreases and with further increasing Q only small changes of $\alpha(Q)$ are found. It is tempting to conclude from this observation that in liquid sodium two different collision regimes have to be considered. Obviously the high- Q regime is essentially determined by "hard-

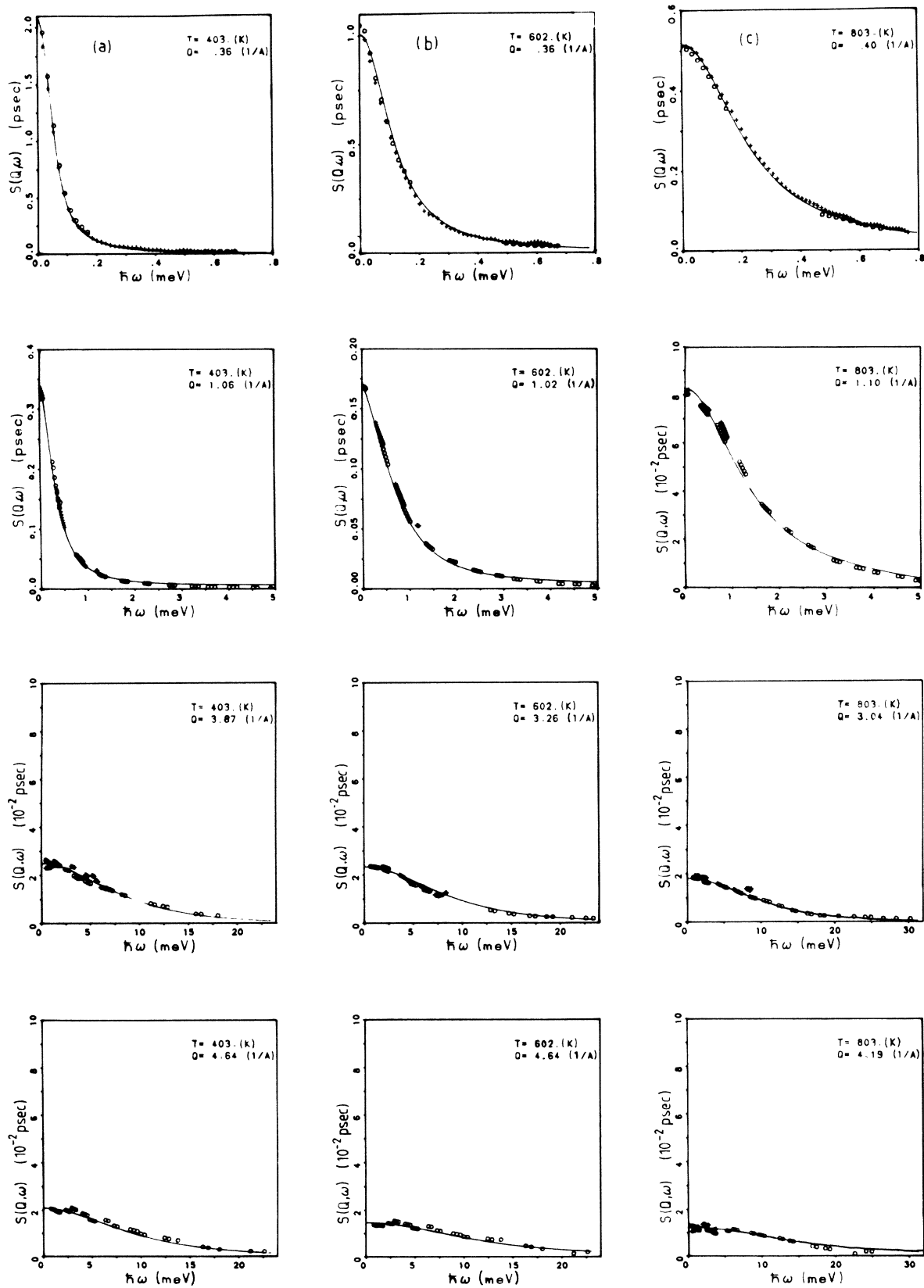


FIG. 3. Typical symmetrized spectra $S_s(Q, \omega)$ at different Q values for the temperatures (a) $T=403$ K, (b) 602 K, and (c) 803 K. [Because of incomplete covering of the kinematic region the Q -sorted experimental $\hat{S}_s(Q, \omega)$ spectra show gaps for small ω regions: +, energy gain; o, energy loss.]

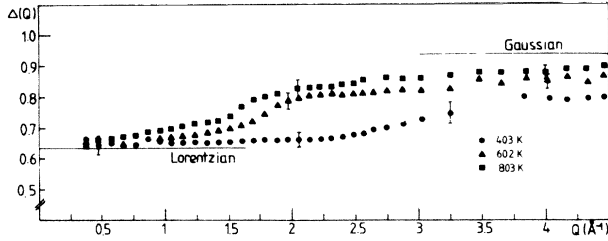


FIG. 4. Q dependence of the product peak width multiplied by peak height $\Delta(Q) = 2\omega_{1/2}(Q)\hat{S}_s(Q, 0)$ at different temperatures. The values for Lorentzians ($\Delta = 2/\pi$) and Gaussians [$\Delta = (4 \ln 2/\pi)^{1/2}$] are indicated at low and high Q , respectively.

sphere-gas"-like behavior, whereas in the low- Q regime more complex collisions typical for diffusive motion behavior are expected. The transition from the low- to the high- Q regime seems to be related to the square root $\omega_0(Q) = Qv_0$ of the second moment of $\hat{S}_s(Q, \omega)$, which can be considered as a characteristic frequency of the system. This simple picture has to be taken with caution, e.g., assuming an ω -independent collision rate is certainly an approximation, which becomes less valid with increasing ω .

A third way to represent Q -dependent shape effects of $\hat{S}_s(Q, \omega)$ is to plot its reduced half-width $\gamma(Q) = \omega_{1/2}(Q)/DQ^2$ as illustrated in Fig. 6. At low Q the de-

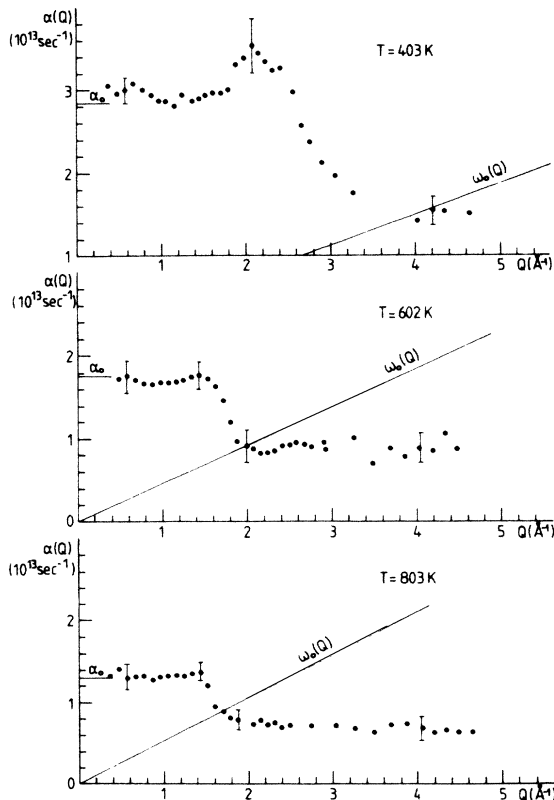


FIG. 5. Collision rate $\alpha(Q)$ as evaluated with the Nelkin-Ghatak model (Ref. 10) at different temperatures [$\alpha_0 = v_0^2/D$ in the hydrodynamic regime; straight line, $\omega_0(Q) = Qv_0$, the typical ideal-gas frequency].

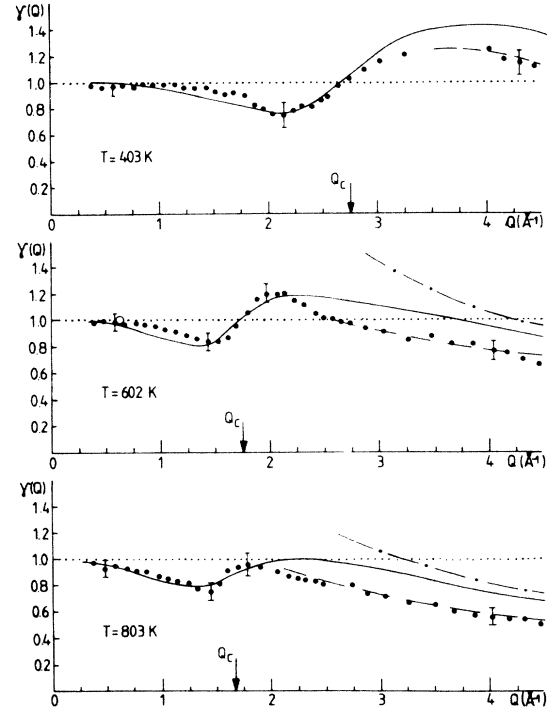


FIG. 6. Reduced half-width $\gamma(Q) = \omega_{1/2}(Q)/DQ^2$ compared at low Q with the classical value $\gamma^{cl}(Q) = 1$ (dotted line) and with the perfect-gas behavior $\gamma(Q) \sim 1/Q$ (for 602 and 803 K) at high Q (dash-dotted curve). Dashed curve, fit to the Enskog theory of a hard-sphere gas (for parameters see Table II); solid curve, theory of Götze and Zippelius (Ref. 7) (for parameters see Table III).

crease of $\gamma(Q)$ with increasing Q relative to its hydrodynamic limit $\gamma(Q \rightarrow 0) = 1$ indicates a diffusion retardation. But then in the transition region pointed out above, the reduced half width increases which reflects an increase in mobility. For $T = 403$ K a comparison with MD calculations⁶ and low Q results^{3,25} show good agreement and finally with growing Q , $\gamma(Q)$ seems to approach the $1/Q$ behavior of the perfect-gas limit. The deviation from the ideal-gas behavior may have to do with the finite hard-core part of the particle potential, which suggests a comparison with the scattering function of an Enskog hard-sphere gas.²⁶ The open parameter of this model, the particle mean free path \bar{l} , can be fitted to the data and on the other hand be directly evaluated using Enskog's prescription: $\bar{l}_E = 1/[\sqrt{2}\pi\sigma^2ng(\sigma)]$, where σ is the hard-sphere diameter^{27,28} and $g(\sigma)$ the pair correlation at contact. The dashed line in Fig. 6 illustrates the fits and Table II

TABLE II. Particle mean-free-path length of liquid sodium at different temperatures.

T (K)	σ (Å)	\bar{l} (Å)	\bar{l}_E (Å)
403	3.26	0.15	0.20
602	3.12	0.26	0.32
803	3.00	0.37	0.45

summarizes the results. The agreement between \bar{l} and \bar{l}_E is rather good, especially if one considers that introducing a hard-sphere mean free path is only an approximation and that at high particle densities this classical length becomes comparable to the thermal wave length of the particle ($T=400$ K, $\lambda_{Na} \approx 0.18$ Å).

Several theoretical models have been proposed in the past to describe the space and time dependence of single-particle motion in liquids^{7,8,29,30}. Among these the models of Lovesey²⁹ and Akcazu *et al.*³⁰ describe the decay of the memory function $M_s(Q,t)$ of the particle's self current correlation by a simple exponential decay, parameterizing the decay or relaxation time $\tau_s(Q)$. Whereas this approximation seems to describe the particle behavior at small Q reasonably, it does not reflect the necessary decrease of $M_s(Q,t)$ at large Q to assure free particle behavior at $Q \rightarrow \infty$. The latter feature has been taken into account in theories of Götze and Zippelius⁷ and Wahnström *et al.*,⁸ which are based on the solution of two coupled kinetic equations for the phase-space density of a fluid particle using the Mori formalism. Because a computer program of the Götze and Zippelius model³¹ was available to us, we compared our data with this model, which has two parameters, namely D and ω_E . A fit of the model's reduced half width $\gamma(Q)$ to the experimental data is also included in Fig. 6. In the low- and intermediate- Q region the observed Q dependence is described quite well. The model explains diffusion retardation at small Q through a Q - and ω -dependent many-particle "potential" created by the motion of the tagged particle which polarizes the surrounding liquid. At a characteristic Q_c value which depends on the temperature this additional effective potential breaks down thus allowing the particle a more free motion which is reflected in the sudden increase of the measured reduced width. The characteristic Q_c of the model can be determined from a least-squares fit to the data, the results are given in Table III and show no evidence for a close connection between Q_c and $Q_0 \approx 2 \text{ Å}^{-1}$, the structure factor maximum.

In the model Q_c is related to the Einstein frequency through the relation $Q_c \approx \omega_E / 2v_0$ leading to the values ω_E^{GZ} quoted in Table III, which we think are in fair agreement with literature values ω_E^L mentioned above, taking the uncertainty of this parameter into account. Whereas the agreement between theory and experiment in the lower- Q region is quite satisfying, Fig. 6 illustrates a systematic difference in the high- Q region. Very probably this effect stems from the fact that the theory does not

TABLE III. Characteristic Q_c values and Einstein frequencies determined from the model fit.

T (K)	Q_c (Å ⁻¹)	ω_E^{GZ} (10 ¹² s ⁻¹)	ω_E^L (10 ¹² s ⁻¹)
403	2.76	21±1.7	16.2
602	1.72	17±1.5	17.0
803	1.67	18±1.5	17.2

take into account a realistic two-particle potential with a repulsive core but rather describes binding via the Einstein frequency ω_E .

V. CONCLUSIONS

We reported a series of inelastic neutron-scattering measurements on liquid sodium at several temperatures which are accurate enough to explore detailed features of the van Hove scattering function. Although in the present case coherent and incoherent scattering had to be separated by a model analysis, the incoherent part which reflects the single-particle motion shows new and interesting features. We think that the results are an excellent test of modern kinetic theories for single-particle motions in liquid metals and indicate directions for further improvement. Further experimental improvement is possible by the use of neutron polarization analysis for the separation of coherent and incoherent scattering. We hope that by applying this technique a more detailed study of the transition region from diffusive to "hard-sphere-gas"-like motion will be feasible.

ACKNOWLEDGMENTS

We gratefully acknowledge the help of Dr. G. Wallner with the sample preparation, the assistance of the workshop of the Forschungs-Reaktor München and the staff of the Institut Laue-Langevin (Grenoble) with the preparation and performance, respectively, of the experiments. We also thank Dr. B. Renker (Kernforschungszentrum Karlsruhe) and Dr. E. Schneider (Universität Ulm) for help with the experiment and data evaluation. We are indebted to Dipl. Phys. J. Lorenz, who made a user version of his $S_s(Q,\omega)$ program available to us. Helpful discussions with Dr. E. Leutheusser and Professor W. Götze are also thankfully acknowledged. This work was supported by the Bundesministerium für Forschung und Technologie (Bonn, Germany).

¹R. Meyer and N. Nachtrieb, *J. Chem. Phys.* **23**, 1852 (1955).

²P. Randolph, *Phys. Rev.* **134**, A1238 (1964).

³S. Cocking, *J. Phys. C* **2**, 2047 (1969).

⁴B. Nijboer and A. Rahman, *Physica* **32**, 415 (1966).

⁵D. Levesque and L. Verlet, *Phys. Rev. A* **2**, 2514 (1970).

⁶T. Kinell, U. Dahlborg, O. Söderström, and I. Ebbsjö, *J. Phys. F* **15**, 1033 (1985).

⁷W. Götze and A. Zippelius, *Phys. Rev. A* **14**, 1842 (1976).

⁸G. Wahnström and L. Sjögren, *J. Phys. C* **15**, 401 (1982).

⁹S. Lovesey, *J. Phys. C* **4**, 3057 (1971).

¹⁰M. Nelkin and A. Ghatak, *Phys. Rev.* **135**, A4 (1964).

¹¹S. Mughabghab, M. Divadeenam, and N. Holden, *Neutron Cross Sections* (Academic, New York, 1981), Vol. I.

¹²*Neutron Research Facilities at the ILL* (Institute Max von Laue—Paul Langevin, Grenoble, France, 1983).

¹³H. Paalman and C. Pings, *J. Appl. Phys.* **33**, 2635 (1962).

- ¹⁴C. Morkel, E. Schneider, and W. Gläser (unpublished).
- ¹⁵J. Copley, *Comput. Phys. Commun.* **7**, 289 (1973).
- ¹⁶V. Sears, *Adv. Phys.* **24**, 1 (1975).
- ¹⁷W. Gläser, R. Gähler, and O. Schärpf, Annex to the Annual Report 1982, ILL Grenoble (unpublished).
- ¹⁸A. Greenfield, J. Wellendorf, and N. Wiser, *Phys. Rev. A* **4**, 1607 (1971).
- ¹⁹A. Rahman, in *Statistical Mechanics: New Concepts, New Problems, New Applications*, edited by S. Rice, K. Freed, and J. Light (University of Chicago, London, 1972), p. 185.
- ²⁰J. Lewis and S. Lovesey, *J. Phys. C* **10**, 3221 (1977).
- ²¹K. Sköld, *Phys. Rev. Lett.* **19**, 1023 (1967).
- ²²*Handbook of Mathematical Functions*, edited by M. Abramowitz and J. Stegun (Dover, New York, 1965).
- ²³P. Egelstaff and P. Schoffield, *Nucl. Sci. Eng.* **12**, 260 (1962).
- ²⁴W. Gläser and C. Morkel, *J. Non-Cryst. Solids* **61& 62**, 309 (1984).
- ²⁵O. Söderström and U. Dahlborg, *J. Phys. F* **14**, 2297 (1984).
- ²⁶V. Sears, *Phys. Rev. A* **5**, 452 (1972).
- ²⁷N. Ashcroft and J. Lekner, *Phys. Rev.* **145**, 83 (1966).
- ²⁸P. Ascarelli and A. Paskin, *Phys. Rev.* **165**, 222 (1968).
- ²⁹S. Lovesey, *J. Phys. C* **6**, 1857 (1973).
- ³⁰A. Akcasu, N. Corngold, and J. Duderstadt, *Phys. Fluids* **13**, 2213 (1970).
- ³¹J. Lorenz, Diplomarbeit, Technische Universität München (1984).